Time-Dependent Viscoelastic Stress Transfer and Earthquake Triggering

Jian Lin

Department of Geology and Geophysics, Woods Hole Oceanographic Institution,

Woods Hole, MA 02543 USA, jlin@whoi.edu tel 508 289 2576 fax 508 457 2187

Andrew M. Freed

Department of Earth & Atmospheric Science, Purdue University,

West Lafayette, IN 47907 USA, freed@purdue.edu tel 765 494 3258 fax 765 496 1210

Abstract. We summarize key features of time-dependent viscoelastic stress transfer following the 1992 M_W=7.3 Landers and M_W=7.1 Hector Mine earthquakes in southern California, for which substantial seismological, geodetic, and geological constraints are available. The 1999 Hector Mine quake occurred only 20 km from but 7 years after the 1992 Landers event, indicating the possibility of time-dependent postseismic stress triggering. We developed 3-D viscoelastic models to simulate stress transfer from the ductile lower crust and/or upper mantle to the brittle upper crust in the 7 years following the 1992 Landers quake. We further derived viscoelastic parameters that can reproduce the observed post-Landers horizontal surface deformation. Our calculations revealed that post-Landers viscous flow in either lower crust or upper mantle can cause postseismic stress increases of up to 1-2 bars at the Hector Mine hypocenter, potentially advancing the occurrence of the 1999 Hector Mine earthquake. Furthermore, the Landers-Hector Mine earthquake sequence has caused significant stress changes on parts of the southern San Andreas and other faults in southern California. For example, the combined coseismic and postseismic stress increase is 2.3–3.5 bars on the San

---

In: *Environment, Natural Hazards, and Global Tectonics of the Earth, ed. Y.J. Chen, Advances in Earth Sciences Monograph, Volume 2*, pp. 21-38, Higher Education Press, Beijing, 2004.

Bernardino Mountain segment of the San Andreas fault during 1992-2002 and such stress increase is projected to be 3.6–4.9 bars by 2020. Similarly, calculations predicted stress buildup on parts of the San Jacinto, Elsinore, and Calico faults in southern California. In particular, the Calico fault, which is located north of the Landers quake, showed post-Landers seismicity and stress buildup patterns that are similar to those observed near the Hector Mine region prior to the 1999 quake. This points to the need to closely monitor the Calico fault. These and other results indicate the potential important role of viscoelastic stress transfer in earthquake triggering.

1. Coulomb Stress Concept

One of the widely used criteria to characterize the conditions under which rock failure occurs is Coulomb failure [*Jaeger and Cook*, 1979]. The calculation of Coulomb stress is based on the geometry (strike/dip/rake, *Aki and Richards*, 2002) and slip of the stress-inducing earthquake (called source earthquake or source fault), the geometry of a receiving fault in the region of interest (called receiver fault), and the apparent coefficient of friction of the crust [e.g., *King et al*., 1994]. The Coulomb failure stress change caused by a source earthquake on an adjacent receiver fault can be expressed as

$$\Delta\sigma_f = \Delta\tau_s + \mu'\Delta\sigma_n, \qquad (1)$$

where $\Delta\tau_s$ is the change in shear stress in the slip direction of the receiver fault, $\Delta\sigma_n$ is the change in normal stress (tension positive), and μ' is the apparent coefficient of friction incorporating the influence of pore pressure. We use the term "apparent" to describe the coefficient of friction because the level of pore pressure, which has a significant influence on the confining pressure, is poorly known in the southern California crust.

If the location and geometry of a received fault are known, such as for a given segment of the San Andreas fault, the Coulomb stress change on the receiver fault can be calculated by resolving the stress tensor of the source quake on the receiver fault. In most cases, however, the location and geometry of the receiver faults are not known and

thus must be assumed. In such cases, one option is to choose the plane on which the Coulomb stress reaches maximum as the plane of failure. For a vertical pure strike-slip fault, by setting both the x and y axes to be horizontal and the z axis to be vertical, we can determine the strike θ of the optimally oriented failure planes from the x-axis through

$$\theta = \phi + \beta, \quad (2)$$

where ϕ is measured from the x axis and can be determined by

$$\phi = 0.5 \tan^{-1}[2\sigma_{xy}/(\sigma_x - \sigma_y)], \quad (3)$$

where σ_{xy} is the total shear stress when considering both the regional and coseismic stresses, and σ_x and σ_y are the total normal stresses. β marks the angle between the failure plane and the maximum compressional stress axis, and is a function of the apparent coefficient of friction μ',

$$\beta = 0.5 \tan^{-1}(1/\mu'). \quad (4)$$

A significant number of studies in recent years have illustrated good correlations between calculated positive coseismic stress changes and the locations of aftershocks [*Stein and Lisowski*, 1983; *Oppenheimer et al*., 1988; *Reasenberg and Simpson*, 1992; *Stein et al.*, 1992; *King et al.*, 1994; *Toda et al.*, 1998]. It was further proposed that Coulomb stress transfer might also trigger moderate to large earthquakes [*King et al.*, 1994; *Stein et al.*, 1994; *Harris et al.*, 1995; *Deng and Sykes*, 1996; *Jaume and Sykes*, 1996; *Stein*, 1999; *Lin and Stein*, 2004]. In this article we summarize the key results of our investigations of the viscoelastic stress relationship between the 1992 Landers and 1999 Hector Mine quakes and their effects on other faults in southern California.

2. Viscoelasticity and Model Geometry

Prior investigations have suggested that postseismic viscous flow in the lower crust or upper mantle can cause significant stress and strain increases in the seismogenic upper crust, causing it eventually to become the main layer to store the strains caused by

an earthquake [*Pollitz and Sacks*, 1995, 1997; *Freed and Lin*, 1998; *Deng et al.*, 1999]. The 1992 Landers and 1999 Hector Mine earthquakes in the Mojave Desert (Figure 1) provide a unique opportunity to investigate the detailed processes of viscoelastic stress transfer and earthquake triggering because relatively abundant seismological, geodetic, and geological constraints are available.

We developed a three-dimensional (3D) viscoelastic model for a wide region of the Mojave Desert (Figure 2) and utilized a modified I-deas finite-element program (see http://www.eds.com) [*Freed and Lin*, 2001]. The lithosphere in the study region is modeled with a Young's modulus E that increases with depth according to the relationship

$$E = (2/3)(1+\nu)\rho V_p^2 \qquad (5)$$

where ν is Poisson's ratio, ρ is density, and V_p is *P*-wave velocity. Based on the seismic reflection results of *Qu et al.* [1994], we divided the lithosphere into a number of layers: E = 3×10^{10} Pa for depth of 0-3 km, E = 5×10^{10} Pa for 3-10 km, E = 7×10^{10} Pa for 10-18 km, E = 1.1×10^{11} Pa for 18-28 km, and E = 1.4×10^{11} Pa below 28 km. We also assumed a Poisson ratio ν of 0.25 for all layers.

Relatively fast regional changes in surface deformation have been observed following the 1992 Landers earthquake through space geodetic measurements [*Shen et al.*, 1994; *Massonnet et al.* 1996; *Savage and Svarc*, 1997; *Jackson et al.*, 1997; *Bock et al.*, 1997]. While a number of mechanisms may have contributed to postseismic surface deformation, e.g., fault zone collapse [*Massonnet et al.* 1996], afterslip [*Shen et al.*, 1994; *Savage and Svarc*, 1997], and poroelastic rebound [*Peltzer et al.*, 2000; *Masterlark and Wang*, 2002], it appears that the observed post-Landers horizontal surface deformation at the time scale of months to years is best explained by viscous flow in either the lower crust [*Ivins*, 1996; *Deng et al.*, 1998] or upper mantle [*Pollitz et al.*, 2000]. Petrological considerations argue that a felsic lower crust is weaker than a mafic upper mantle [*Kirby and Kronenberg*, 1987], thus favoring viscous flow in the lower crust. On the other hand,

the limited observations of post-Landers vertical surface deformation appear to be better explained by models of viscous flow in the upper mantle [*Pollitz et al.*, 2000]. We thus consider viscous flow in either the lower crust or upper mantle. In the following we first illustrate the coseismic stress patterns of the 1992 Landers quake, to be followed by a description of the role of postseismic viscoelastic stress transfer in triggering the 1999 Hector Mine quake. We then illustrate the effects of the Landers and Hector Mine events on the southern San Andreas and other faults in southern California. In most cases, a range of values for the apparent friction coefficient, from low (μ'=0.2) to intermediate (μ'=0.5) to high (μ'=0.8), were examined to test the sensitivity of model results.

3. Coseismic Stress Changes by the 1992 Landers Quake

The June 1992 M_W=7.3 Landers event was the largest earthquake in southern California in several decades. It was preceded by the April 1992 M_W=6.1 Joshua Tree quake and followed by the M_W=6.2 Big Bear major aftershock only three and half hours later [*Hauksson et al.*, 1993] (Figure 1). To accurately model the Landers source fault, we used the results of Landers rupture distribution from the joint inversion of seismic travel time, waveform, and geodetic data [*Wald and Heaton*, 1994]. We mapped the inferred Landers slip distribution onto fault geometry according to the observed surface breaks [*Hauksson et al.*, [1993] (Figure 2c).

The regions of calculated coseismic Coulomb stress increase spread out in a butterfly-shaped pattern over a large area in southern California (Figure 3). Within a few months after the Landers quake, a group of aftershocks were observed near the future Hector Mine epicenter. The occurrence of such aftershock cluster suggests that the crust near the future Hector Mine epicenter was probably already weak in 1992. Although the Landers coseismic stress changes might not be sufficient to trigger the Hector Mine quake itself, the triggering threshold was likely to be close. The calculated

Coulomb stress results show reasonable agreement with the aftershock locations for assumed apparent friction in the range of $0.2<\mu'<0.6$. Furthermore the predicted coseismic horizontal displacement vectors show good agreement with those determined by GPS and trilateration measurements [*Wald and Heaton*, 1994] (Figure 4a).

To further illustrate the effects of the Landers quake on the Hector Mine region, we calculated models in which the receiver faults are assumed to be right-lateral and have the same strike as the observed Hector Mine surface rupture (N20°W) (Figure 6). The calculations reveal that the Hector Mine hypocenter is located in a narrow stripe of positive coseismic Coulomb stress changes and this small positive area is surrounded both to the north and south by wide regions of negative coseismic stress changes (Figure 6a). We noted, however, that small changes in the assumed Landers slip distribution, its rupture geometry, or apparent friction can move the calculated area of positive stress changes by several kilometers. Such sensitivity to the assumed model parameters illustrates that the coseismic stress changes caused by the 1992 Landers quake on the future Hector Mine hypocenter are relatively small. This sensitivity also explains the apparent lack of a consensus among various models on the sign and magnitude of the calculated coseismic stress changes at the future Hector Mine hypocenter [e.g., *USGS et al.*, 2000; *Parsons and Dreger*, 2000].

4. Viscoelastic Stress Changes in the 1999 Hector Mine Epicenter Region

We used the observed surface deformation following the Landers quake to constrain the viscoelastic parameters in our stress models. We found that models of viscous flow in either the lower crust or upper mantle can reproduce reasonably well the observed horizontal deformations in both the far-field (*Southern California Earthquake Center*, 2001; Figure 4b) and near-field regions (*Savage and Svarc*, 1997; Figures 4c, 4d, 5) during October 1992 to December 1995. Similarly, the observed accumulated horizontal deformation at the USGS GPS station OLDW from October 1992 to January 1998 [*Savage*

and Svarc, 1997, *Prescott*, 2001] is matched reasonably well by models of viscous flow in either the lower crust or upper mantle (Figure 4e). For the lower crustal flow model, the calculated best-fitting viscosity is $\eta=3 \times 10^{18}$ Pa·s for a viscous layer in the lower crust at depth of 18-28 km. For the upper mantle flow model, the best-fitting viscosity values are $\eta=5 \times 10^{18}$ Pa·s for depth of 28–50 km and $\eta=3 \times 10^{18}$ Pa·s for depth of 50–120 km.

The 1992 Landers quake has caused a large lobe of positive coseismic Coulomb stress changes in the lower crust and upper mantle of the Hector Mine region (Figure 6a). If either the lower crust or upper mantle is viscous and thus unable to sustain this stress load during the months and years following the Landers quake, this deep lobe of coseismic Coulomb stress increase must migrate into the brittle upper crust as the lower crust or upper mantle relaxes. The rate of such stress migration depends directly on the viscosity of the lower crust and upper mantle of the Mojave Desert. For the model of viscous flow in the lower crust, we calculated that the postseismic Coulomb stress increase at the Hector Mine hypocenter is up to 1 bar during 1992-1999 (Figures 6c and 7). For the viscous upper mantle flow case, the calculated postseismic stress increase at the Hector Mine hypocenter is up to 2 bars during 1992-1999 (Figures 6e and 7). Thus the postseismic stress changes provide a viable mechanism for explaining the delayed triggering of the Hector Mine earthquake. The calculated evolution of Coulomb stresses along the Hector Mine cross section as a function of time is further illustrated in Figure 11.

The calculated postseismic stress changes following the Landers quake seems to correlate with the spatial extent of the 1999 Hector Mine rupture zone. Along the Hector Mine rupture plane, the region of calculated postseismic stress increase extends over the two-third and full length, respectively, of the eventual Hector Mine rupture surface in models of viscous flow in the lower crust (Figure 6c) and upper mantle (Figure 6e). Meanwhile, the combined coseismic and postseismic stress changes remained negative near and beyond the lateral ends of the Hector Mine rupture surface (Figures 6b and 6d).

The above correlation raised an interesting possibility that the extent of the Hector Mine rupture zone might be influenced by the region of combined coseismic and postseismic stress changes. However, it is also possible that such apparent correlation is coincidental and that the actual rupture extent of the Hector Mine quake was controlled by other factors such as earthquake dynamic rupture processes or mechanical heterogeneity in the crust.

5. Coseismic Stress Changes by the 1999 Hector Mine Quake

When modeling the stresses associated with the 1999 M_W=7.1 Hector Mine earthquake, we used the detailed slip distribution inferred from the inversion of traveltime and waveform records of regional and local seismic stations [*Dreger and Kaverina,* 2000]. This slip distribution was assumed to be purely right-lateral strike-slip and was mapped onto a vertical plane with geometry based on observed surface ruptures. We found good correlation between the observed GPS coseismic horizontal deformation [*Agnew et al.,* 2002] and that calculated for the Hector Mine earthquake by our model (Figure 4f). Most of the Hector Mine aftershocks appear to be confined within a narrow stripe that is roughly N-S oriented and over areas of calculated stress increases (Figure 8b).

6. Stress Changes on the San Andreas Fault by the Landers-Hector Mine Quakes

The Mojave, San Bernardino Mountain, and Coachella Valley segments of the San Andreas fault (Figure 1) lie within the region of static stress influence of the 1992 Landers and 1999 Hector Mine earthquakes. All of these three segments of the southern San Andreas fault are capable of producing M_W>7.5 major earthquakes [*Working Group on California Earthquake Probabilities*, 1988]. Paleoseismicity studies indicated that the last major earthquake on the Mojave segment was in 1857 and the estimated repeat time of major quakes is about 130 yr and the San Bernardino Mountain segment last ruptured in

1812 [*Jacoby et al.,* 1988; *Sieh et al.,* 1989]. The Coachella Valley segment last ruptured in 1680 with a repeat time of >235 yr [*Sieh,* 1986; *Stein et al.,* 1992]. While recognizing that the estimated repeat times of these fault segments are associated with large uncertainties, it is possible that these fault segments might be late in their earthquake cycle. Thus even relatively small stress increases on these fault segments may be sufficient to trigger a major earthquake.

We illustrate the evolution of coseismic and postseismic stress changes on the southern San Andreas fault and surrounding region in Figures 9. The examples shown are for calculations assuming that the receiver faults have a strike of N60°W and have relatively low values of apparent friction (μ'=0.2) based on the previous studies that argued that the San Andreas is relatively weak [*Zoback et al.,* 1987; *Harris et al.* 1995; *Parsons et al.,* 1999; *Toda and Stein,* 2002]. Our detailed solutions reveal that the calculated coseismic Coulomb stress increases could reach up to 1.8 bars along the central part of the San Bernardino Mountain segment (assuming a strike of N60°W) and 3 bars in the San Gorgonio pass area (assuming a strike of N85°W). In contrast, calculations reveal a stress decrease of 1.5 bars along the western edge of the Coachella Valley segment (assuming a strike of N50°W) and a decrease of 0.5 bars on the Mojave segment (assuming a strike of N65°W) (Figures 9a and b).

Most importantly the calculation results suggest that postseismic stresses continue to build up on parts of the southern San Andreas fault years after the Landers and Hector Mine quakes. The calculated combined coseismic and postseismic stress changes during 1992-2001 are shown in Figures 9c and d for a model of viscous flow in the upper mantle with low apparent friction (μ'=0.2) and a strike of N60°W for receiver faults. Along the San Bernardino Mountain segment, the region of stress increase (red area) in the brittle upper crust is calculated to have spread from a 40-km-wide zone immediately after the 1992 earthquakes (Figures 9b) to a 70-km-wide zone by 2001 (Figures 9d). This zone of stress increase is calculated to further grow to 85 km wide by

2020 (Figures 9f). Some recent preliminary studies have suggested that the stress-strain rate relationship for the crust and mantle may be non-linear with the effective viscosity increasing with time as stresses diminish [*Pollitz et al.,* 2001]. Thus the stress results from our models of uniform viscosity should be considered upper bounds and may have over predicted the rate of stress changes for later years.

The calculated evolution of Coulomb stress changes as a function of time within the central San Bernardino Mountain and western Coachella Valley segments is further illustrated in Figure 10. The solutions were obtained for models of viscous flow in the lower crust and upper mantle and for assumed apparent friction of μ'=0.2, 0.5, and 0.8, respectively. These results show that the calculated pattern of stress evolution in the brittle upper crust is not overly sensitive to whether postseismic viscous flow occurs in the lower crust or upper mantle. The San Bernardino Mountain segment is calculated to have a projected stress increase of 3.6-4.9 bars by 2020. In contrast, the Mojave segment is predicted to be associated with a stress decrease of 1.5 bars by 2020. Meanwhile, the calculated stress changes on the Coachella Valley segment are very sensitive to the assumed apparent friction: the stress changes are negative for the low and immediate values of apparent friction (μ'=0.2 and 0.5) but are positive for the high friction case (μ'=0.8). The calculated stress evolution along the southern San Andreas fault as a function of time is further illustrated in Figure 12.

7. Stress Changes on Other Faults in Southern California

In addition to the San Andreas fault, several other fault systems in southern California also lie within the region of static stress influence of the Landers and Hector Mine earthquakes, including the San Jacinto and Elsinore fault zones that are located close to the Los Angeles and San Diego areas and are capable of producing M_W=6.5–7 earthquakes [*Anderson et al.*, 1989; *Rockwell et al*., 1990; *Sanders and Magistrale,* 1997]. We calculated that Coulomb stress increase could reach up to 3 bars by 2020 on a portion of

the San Jacinto fault that last ruptured in 1899 during an M_W=6.7 quake [*Hanks et al.*, 1975] (Figure 9e). Meanwhile, the northern part of the Elsinore fault is calculated to be associated with a stress increase of about 1 bar by 2020 (Figure 9e).

To the north of the Landers rupture zone, the Calico, Lenwood, and Blackwater faults all lie within the distance of stress influence of the Landers and Hector Mine quakes (Figure 9). We calculated Coulomb stress increases of up to 3 bars on the northern part of the Calico fault and the southern edge of the Blackwater fault by 2020 (Figure 9e). Immediately after the 1992 Landers quake, clusters of aftershock were observed near the Calico fault [*Hauksson et al.*, 1993], suggesting that part of the Calico fault might be close to failure. This pattern of aftershock clustering is similar to that noticed in the Hector Mine epicenter region prior to the 1999 earthquake. Furthermore our calculations suggest that Coulomb stresses on parts of the Calico fault continue to increase due to postseismic viscous relaxation of the lower crust or upper mantle (Figures 9a, c, and e). Thus the Calico fault warrants close monitoring. In contrast, the southern part of the Lenwood fault is in a region of calculated stress decrease (Figure 9).

8. Conclusions

Our calculations revealed that during the 7 years after the 1992 Landers quake, viscous relaxation of the lower crust or upper mantle in the Mojave Desert may have caused postseismic stress increases of up to 1-2 bars at the Hector Mine hypocenter, potentially advancing the occurrence of the 1999 Hector Mine earthquake. The Landers and Hector Mine quakes in turn are calculated to have caused significant stress changes on parts of the southern San Andreas and other faults in southern California. Both the San Bernardino Mountain segment of the San Andreas fault and the Calico fault north of the Landers region are calculated to be undergoing stress buildup since 1992. The San Bernardino Mountain segment is capable of producing large earthquakes and may be relatively late in its quake cycle, while the Calico fault has shown post-Landers

seismicity pattern similar to that observed in the Hector Mine epicenter region prior to the 1999 Hector Mine quake. Thus both the San Bernardino Mountain segment and the Calico fault warrant particular attention. We argue that viscoelastic stress transfer in the lower crust and upper mantle could potentially play an important role in earthquake triggering.

Acknowledgements. This review article summarizes key findings of our investigation of the 1992 Landers and 1999 Hector Mine earthquakes and expands on the earlier results of *Freed and Lin* [2001, 2002]. We are grateful to constructive reviews by J. Chen and Z. Zhu. This work is supported by National Science Foundation through grant EAR-0003888 (Jian Lin) and EAR-0122868 (Andrew Freed).

References

Agnew, D.C., S. Owen, Z.-K. Shen, G. Anderson, J. Svarc, H. Johnson, K.E. Austin, and R. Relinger, Coseismic displacements from the Hector Mine earthquake: Results from Survey-Mode Global Positioning System measurements, *Bull. Seismo. Soc. Amer.,* 92, 1355-1364, 2002.

Aki, K., and P.G. Richards, *Quantitative seismology*, 2nd Edition, University Science Books, pp. 700, 2002.

Anderson, J.G., T.K. Rockwell, and D.C. Agnew, Past and possible future earthquakes of significance to the San Diego region, *Earthq. Spectra, 5*, 299–333, 1989.

Bock, Y. S. Wdowinski, P. Fang, J. Zhang, S. Williams, H. Johnson, J. Behr, J. Genrich, J. Dean, M. van Domselaar, D. Agnew, F. Wyatt, K. Stark, B. Oral, K. Hudnut, R. King, T. Herring, S. Dinardo, W. Young, D. Jackson, W. Gurtner, Southern California permanent GPS geodetic array: Continuous measurements of regional crustal deformation between the 1992 Landers and 1994 Northridge earthquakes, *J. Geophys. Res., 102,* 18013-18033, 1997.

Deng, J., and L.R. Sykes, Triggering of 1812 Santa Barbara earthquake by a great San Andreas shock: Implications for future seismic hazards in southern California, *Geophys. Res. Lett., 23*, 1155-1158, 1996.

Deng, J., M. Gurnis, H. Kanamori, and E. Hauksson, Viscoelastic flow in the lower crust after the 1992 Landers, California, earthquake, *Science, 282*, 1689–1692, 1998.

Deng, J., K. Hudnut, M. Gurnis, and E. Hauksson, Stress loading from viscous flow in the lower crust and triggering of aftershocks following the 1994 Northridge, California, earthquake, *Geophys. Res. Lett.*, *26*, 3209–3212, 1999.

Dreger, D., and A. Kaverina, Seismic remote sensing for the earthquake source process and near source strong shaking, A case study of the October 16, 1999 Hector Mine Earthquake, *Geophys. Res. Lett.*, *27*, 1941–1944, 2000.

Freed, A.M., and J. Lin, Time-dependent changes in failure stress following thrust earthquakes, *J. Geophys. Res.*, *103*, 24,393–24,409, 1998.

Freed, A.M., and J. Lin, Delayed triggering of the 1999 Hector Mine earthquake by viscoelastic stress transfer, *Nature, 411*, 180–183, 2001.

Freed, A.M., and J. Lin, Accelerated stress buildup on the Southern San Andreas Fault and surrounding regions caused by Mojave Desert earthquakes, *Geology*, *30,* 571-574, 2002.

Hanks, T.C., J.A. Hileman, and W. Thatcher, Seismic moment of the largest earthquakes of the southern California region, *Geol. Soc. Amer. Bull., 86*, 1131–1139, 1975.

Harris, R.A., and R.W. Simpson, Changes in static stress on southern California faults after the 1992 Landers earthquake, *Nature, 360*, 251–254, 1992.

Harris, R.A., R.W. Simpson, and P.A. Reasenberg, Influence of static stress changes on earthquake locations in southern California, *Nature, 375*, 221-224, 1995.

Hauksson, E., L.M. Jones, K. Hutton, D. Eberhart-Phillips, The 1992 Landers earthquake sequence: Seismological observations, *J. Geophys. Res., 98*, 19,835–19,858, 1993.

Ivins, E.R., Transient creep of a composite lower crust, 2. A polymineralic basis for rapidly evolving postseismic deformation modes, *J. Geophys. Res*., *101*, 28,005-28,028, 1996.

Jackson, D.D., Z.K. Shen, D. Potter, X.B. Ge, and L.Y. Sung, Geoscience: Southern California deformation, *Science, 277*, 1621-1622, 1997.

Jacoby, G.C.Jr., P.R. Shepard, and K.E. Sieh, Irregular recurrence of large earthquakes along the San Andreas fault in southern California - Evidence from trees near Wrightwood, *Science, 241*, 196–199, 1988.

Jaeger, J. C., and N. G. W. Cook, *Fundamentals of Rock Mechanics*, 3rd ed., Chapman and Hall, New York, 1979.

Jaume, S.C., and L.R. Sykes, Evolution of moderate seismicity in the San Francisco Bay region, 1850 to 1993: seismicity changes related to the occurrence of large and great earthquakes, *J. Geophys. Res*., *101*, 765-789, 1996.

King, G.C.P., R.S. Stein, and J. Lin, Static stress changes and the triggering of earthquakes, *Bull. Seismo. Soc. Amer*., *84*, 935–953, 1994.

Kirby, S.H., and A.K. Kronenberg, Rheology of the lithosphere: Selected topics, *Rev. Geophys*., *25*, 1219-1244, 1987.

Lin, J., and R.S. Stein, Stress triggering in thrust and subduction earthquakes and stress interaction between the Southern San Andreas and nearby thrust and strike-slip faults, *J. Geophys. Res., 109,* B02323, doi:10.1029/2003JB002607, 2004.

Massonnet, D., W. Thatcher, and H. Vadon, Detection of postseismic fault-zone collapse following the Landers earthquake, *Nature, 382*, 612-616, 1996.

Masterlark, T., and H.F. Wang, Transient stress-coupling between the 1992 landers and 1999 Hector Mine, California, earthquakes, *Bull. Seismo. Soc., Amer., 92*, 1470-1486, 2002.

Oppenheimer, D.H., P.A. Reasonberg, and R.W. Simpson, Fault plane solutions for the 1984 Morgan Hill, California, earthquake sequence: Evidence for the state of stress on the Calavares fault, *J. Geophys. Res., 93*, 9007–9026, 1988.

Parsons, T., R.S. Stein, R.W. Simpson, and P.A. Reasenberg, Stress sensitivity of fault seismicity: A comparison between limited-offset oblique and major strike-slip faults, *J. Geophys. Res., 104*, 20,183-20,202, 1999.

Parsons, T., and D.S. Dreger, Static-stress impact of the 1992 Landers earthquake sequence on nucleation and slip at the site of the 1999 M=7.1 Hector Mine earthquake, southern California, *Geophys. Res. Lett., 27*, 1949-1952, 2000.

Peltzer, G., P. Rosen, F. Rogez, and K. Hudnut, Poro-elastic rebound along the Landers 1992 earthquake surface rupture, *J. Geophys. Res., 103*, 30,131-30,145, 1998.

Pollitz, F.F., and I.S. Sacks, Consequences of stress changes following the 1891 Nobi earthquake, Japan, *Bull. Seismo. Soc. Amer., 85*, 796–807, 1995.

Pollitz, F.F., and I.S. Sacks, The 1995 Kobe, Japan, earthquake: A long-delayed aftershock of the offshore 1944 Tonankai and 1946 Nankaido earthquakes, *Bull. Seismo. Soc. Amer., 87*, 1–10, 1997.

Pollitz, F.F., and I.S. Sacks, Stress triggering of the 1999 Hector Mine earthquake by transient deformation following the 1992 Landers earthquake, *Bull. Seismo. Soc. Amer.*, 92, 1487-1496, 2002.

Pollitz, F.F., G. Peltzer, and R. Bürgmann, Mobility of continental mantle: Evidence from postseismic geodetic observations following the 1992 Landers earthquake, *J. Geophys. Res., 105*, 8035–8054, 2000.

Pollitz, F.F., C. Wicks, and W. Thatcher, Mantle flow beneath a continental strike-slip fault: Postseismic deformation after the 1999 Hector Mine earthquake, *Science, 293*, 1814–1817, 2001.

Prescott, W., 2001, Post-Landers GPS data: http://ncwebalt-menlo.wr.usgs.gov/research/deformation/gps/auto/LandersPro, (May, 2001).

Qu, J., T.L. Teng, and J. Wang, Modeling of short-period surface wave propagation in southern California, *Bull. Seismo. Soc. Amer., 84*, 596–612, 1994.

Reasenberg, P.A., and R.W. Simpson, Response of regional seismicity to the static stress change produced by the Loma Prieta earthquake, *Science, 255*, 1687-1690, 1992.

Rockwell, T.C., C. Loughman, and P. Merifield, Late quaternary of slip along the San Jacinto zone near Anza, southern California, *J. Geophys. Res., 95*, 8593–8605, 1990.

Sanders, C., and H. Magistrale, Segmentation of the northern San Jacinto fault zone, southern California, *J. Geophys. Res., 102*, 27,453-27,467, 1997.

Savage, J.C., and J.L. Svarc, Postseismic deformation associated with the 1992 M_W=7.3 Landers earthquake, southern California, *J. Geophys. Res., 102*, 7565–7577, 1997.

Shen, Z., D.D. Jackson, Y. Feng, M. Cline, M. Kim, P. Fang, and Y. Bock, Postseismic deformation following the Landers earthquake, California, 28 June 1992, *Bull. Seismo. Soc. Amer., 84*, 780-791, 1994.

Southern Californian Earthquake Center (SCEC), 2001, Horizontal deformation velocity field, version 2.0: http://www.scecdc.scec.org:3128/group_e/release.v2 (May, 2001).

Sieh, K.E., Slip rate across the San Andreas fault and prehistoric earthquakes at Indio, California, *EOS Trans. AGU, 67*, 1200, 1986.

Sieh, K.E., M. Stuiver, and D. Brillinger, A more precise chronology of earthquakes produced by the San Andreas fault in southern California, *J. Geophys. Res., 94*, 603–623, 1989.

Stein, R.S., The role of stress transfer in earthquake occurrence, *Nature, 402*, 605–609, 1999.

Stein, R.S., and M. Lisowski, The 1979 Homestead Valley earthquake sequence, California: Control of aftershocks and postseismic deformation, *J. Geophys. Res., 88*, 6477–6490, 1983.

Stein, R.S., G.C.P. King, and J. Lin, Change in failure stress on the southern San Andreas fault system caused by the 1992 magnitude=7.4 Landers earthquake, *Science, 258*, 1328–1332, 1992.

Stein, R.S., G.C.P. King, and J. Lin, Stress triggering of the 1994 M=6.7 Northridge, California, earthquake by its predecessors, *Science, 265*, 1432-1435, 1994.

Toda, S., R.S. Stein, P.A. Reasonberg, and J.H. Dieterich, Stress transferred by the M_W=6.5 Kobe, Japan, shock: Effect on aftershocks and future earthquake probabilities, *J. Geophys. Res., 103*, 24543-24565, 1998.

Toda, S., and R.S. Stein, Response of the San Andreas fault to the 1983 Coalinga-Nuñez Earthquakes: An application of interaction-based probabilities for Parkfield, *J. Geophys. Res., 107*, 10.1029/2001JB000172, 2002.

U.S. Geological Survey, Southern Californian Earthquake Center, and California Division of Mines and Geology, Preliminary report on the 16 October 1999 M 7.1 Hector Mine, California, earthquake, *Seismo. Res. Lett., 71*, 11–23, 2000.

Wald, D.J., and T.H. Heaton, Spatial and temporal distribution of slip for the 1992 Landers, California, earthquake, *Bull. Seismo. Soc. Amer., 84*, 668–691, 1994.

Working Group on Californian Earthquake Probabilities (WGCEP), *U.S. Geological Survey, Open-File Report*, 88–396, 1988.

Zoback, M.D., M.L. Zoback, V.S. Mount, J. Suppe, J.P. Eaton, J.H. Healy, D.H. Oppenheimer, P.A. Reasenberg, L.M. Jones, C.B. Raleigh, I.G. Wong, O. Scotti, and C.M. Wentworth, New evidence on the state of stress of the San Andreas fault system, *Science, 238*, 1105-1111, 1987.

Figure Caption

Figure 1. Map showing the southern San Andreas and other faults in the Mojave Desert. Also shown are four significant earthquakes during 1992-1999 with the circle size proportional to earthquake magnitude. Marked cities: B—Barstow, SB—San Bernardino, PS—Palm Springs, P—Palmdale, and CP—Cajon Pass.

Figure 2. (a) We used a cylindrical viscoelastic finite element model to calculate Coulomb stress changes caused by the 1992 Landers and 1999 Hector Mine earthquakes. (b) Detailed fault geometry in the center of the model domain. (c) We explicitly used the observed slip distribution of *Wald and Heaton* [1994] to specify the Landers rupture.

Figure 3. (a) Correspondence between the calculated coseismic Coulomb stress changes caused by the 1992 Landers earthquake sequence (color) and the seismicity ($M_W > 3$, dots) observed during a period from immediately after the Landers quake (June 28, 1992) to right before the Hector Mine event (October 16, 1999). Black lines denote faults that ruptured in 1992: Landers (L), Big Bear (BB), and Joshua Tree (JT). All quakes are right-lateral strike slip except for the Big Bear quake that is left lateral. Black on yellow line marks the location of the future 1999 Hector Mine (HM) quake with the epicenter shown as a star. Dashed line shows the San Andreas (SA) fault. The stresses are shown for example calculations assuming apparent coefficient of friction $\mu'=0.4$. We calculated the orientations of receiver faults by considering both coseismic stresses and a 100 bar regional compressional stress field with its maximum compression axis at N7°E [*Stein et al.,* 1992; *King et al.,* 1994]. (b) Details of the rupture segments in the northern Landers region: CR—Camp Rock, E—Emerson, and HV—Homestead Valley. Dotted lines show the potential buried E-W rupture surfaces inferred from the study of *Dreger and Kaverina* [2000].

Figure 4. (a) Observed GPS coseismic horizontal surface deformation [*Wald and Heaton*, 1994] and calculated surface deformation from our Landers coseismic model. (b) Observed far-field postseismic (October 1992 to December 1995) horizontal surface deformation from GPS measurements [*SCEC*, 2001] and calculated postseismic deformation from models of viscous flow in the lower crust or upper mantle. (c) Observed GPS near-field postseismic (October 1992 to December 1995) horizontal deformation along USGS Emerson transect [*Savage and Svarc*, 1997] and calculated deformation. (d) Magnitude of observed GPS near-field postseismic (October 1992 to December 1995) horizontal deformation along the USGS Emerson transect (circles) [*Savage and Svarc*, 1997] and that predicted by lower crustal flow models with assumed lower crustal viscosity values of $1x10^{18}$ Pa s (short dashed line), $3x10^{18}$ Pa s (solid line), and $5x10^{18}$ Pa s (long dashed line), respectively. (e) Observed accumulated deformation at GPS station OLDW from October 1992 to January 1998 (circles) [*Savage and Svarc*, 1997; *Prescott*, 2001] and accumulated deformation predicted by models of viscous flow in the lower crust or upper mantle. (f) Observed GPS coseismic horizontal surface deformation associated with the 1999 Hector Mine quake [*Agnew et al.*, 2002] and that predicted by our coseismic models for the Hector Mine quake. Marked fault segments in (a)-(c) and (f): L—Landers, BB—Big Bear, JT—Joshua Tree, HM—Hector Mine, and SA—San Andreas fault.

Figure 5. Observed GPS near-field postseismic (October 1992 to December 1995) horizontal deformation along the USGS Emerson transect (circles) [*Savage and Svarc*, 1997] and that predicted by lower crustal flow models with assumed lower crustal viscosity values of $2x10^{18}$ Pa s (short dashed line), $4x10^{18}$ Pa s (solid line), and $6x10^{18}$ Pa s (long dashed line), respectively. The displacements were resolved into components that

are normal (a) and parallel (b), respectively, to the overall trend of the Landers rupture zone. The location of transect is shown in Figure 4c.

Figure 6. (a) Calculated coseismic Coulomb stress changes caused by the 1992 Landers earthquake sequence. Stresses are shown both for the top ground surface and for a cross section along the rupture surface of the future Hector Mine earthquake (defined by black within yellow line). Black star shows the future Hector Mine hypocenter. White lines on the top ground surface show the 1992 ruptures: Joshua Tree (JT), Landers (L), and Big Bear (BB). Calculations were made assuming that the receiver faults have the same orientation as the Hector Mine rupture zone (N20°W) and that the apparent friction is relatively high (μ'=0.8) as inferred from *Parsons and Dreger* [2000]. (b) Calculated combined coseismic and 7 years of postseismic Coulomb stress changes for a model of viscous flow in the lower crust. (c) Calculated postseismic Coulomb stress changes caused solely by lower crustal viscous flow during 1992-1999. (d) Calculated combined coseismic and 7 years of postseismic Coulomb stress changes for a model of viscous flow in the upper mantle. (e) Calculated postseismic Coulomb stress changes caused solely by upper mantle viscous flow during 1992-1999

Figure 7. Calculated Coulomb stress changes at the Hector Mine hypocenter as a function of time for various assumed values of apparent friction and for models of viscous flow in the lower crust (a) and upper mantle (b). Note that all models suggest increases in postseismic Coulomb stress with time at the Hector Mine hypocenter.

Figure 8. (a) Calculated coseismic Coulomb stress changes caused by the 1999 Hector Mine earthquake. (b) Calculated combined coseismic and postseismic stress changes caused by the 1992 Landers and 1999 Hector Mine quakes as well as viscous flow in the lower crust during 1992-2000. Aftershocks ($M_W > 3$) that occurred following the October,

1999 Hector Mine quake through July 2000 are shown as white circles. Receiver fault orientations were calculated considering both coseismic stresses and a regional stress field with its maximum compression axis at N7°E [*Stein et al*., 1992; *King et al*., 1994]. Stresses shown are for example calculations assuming apparent coefficient of friction $\mu'=0.4$. The color scale of the calculated stress changes is similar to that of Figure 3. Marked faults: L—Landers; HM—Hector Mine; JT—Joshua Tree; BB—Big Bear; SA—San Andreas.

Figure 9. (a) Map showing calculated coseismic Coulomb stress changes caused by the 1992 ruptures (white solid lines): JT—Joshua Tree, L—Landers, and BB—Big Bear. Black and while dashed lines mark the San Andreas fault: MS—Mojave segment, SBMS—San Bernardino Mountain segment, and CVS—Coachella Valley segment. White dashed line denotes the future 1999 Hector Mine (HM) rupture zone. Black lines show other faults in the region: SJF—San Jacinto, EF—Elsinore, CF—Calico, LF—Lenwood, and BWF—Blackwater. (b) Same as panel a but stresses are shown for top surface and a cross section (front) along the San Andreas fault. Stars in the cross section indicate the San Bernardino Mountain and Coachella Valley segments, respectively, where stresses are sampled for Figure 10. (c), (e): Same as panel a but with addition of coseismic stress changes caused by the 1999 Hector Mine earthquake and postseismic relaxation during periods of 1992-2001 and 1992-2020, respectively. Postseismic stress calculations shown in this figure are for a model of viscous flow in the upper mantle. (d), (f): Same as panels c and e, respectively, but stresses are shown for top surface and a cross section (front) along the San Andreas fault. Receiver faults are assumed to strike N60°W. The apparent coefficient of friction is assumed to be relatively low ($\mu'=0.2$) since prior investigations have suggested that the San Andreas fault is relatively weak [*Zoback et al.*, 1987; *Harris et al.* 1995; *Parsons et al.*, 1999; *Toda and Stein,* 2002].

Figure 10. Calculated Coulomb stress changes on the San Bernardino Mountain segment (a) and Coachella Valley segment (b) of the San Andreas fault as a function of time since 1992. The stress sampling locations are shown as stars in Figure 9b. Calculations are shown for coseismic stress changes caused by the 1992 Landers and 1999 Hector Mine earthquakes as well as postseismic stress changes for models of viscous flow in the lower crust and upper mantle, respectively. Results are shown for various assumed apparent friction, corresponding to weak (μ'=0.2), intermediate (μ'=0.5), and strong (μ'=0.8) fault models. All calculations assumed strike directions of N60°W for the San Bernardino Mountain segment and N50°W for the Coachella Valley segment.

Figure 11. Calculated combined coseismic and postseismic changes in Coulomb stress in the vicinity of the Hector Mine region for a model of viscous flow in the lower crust. All calculations assumed the Hector Mine fault is relatively strong with apparent friction μ'=0.8 as inferred from *Parsons and Dreger* [2000]. Results are shown for (a) right after the 1992 Landers quake, (b) 1993, (c) 1995, (d) 1997, and (e) immediately before the 1999 Hector Mine quake.

Figure 12. Calculated combined coseismic and postseismic changes in Coulomb stress in the vicinity of the San Andreas fault for a model of viscous flow in the upper mantle. All calculations assumed the San Andreas fault is relatively weak with apparent friction μ'=0.2 as inferred from prior studies [*Zoback et al.*, 1987; *Harris et al.* 1995; *Parsons et al.*, 1999; *Toda and Stein*, 2002]. Results are shown for (a) right after the 1992 Landers quake, (b) immediately before the 1999 Hector Mine quake, (c) 2000, and (d) projection to 2022.

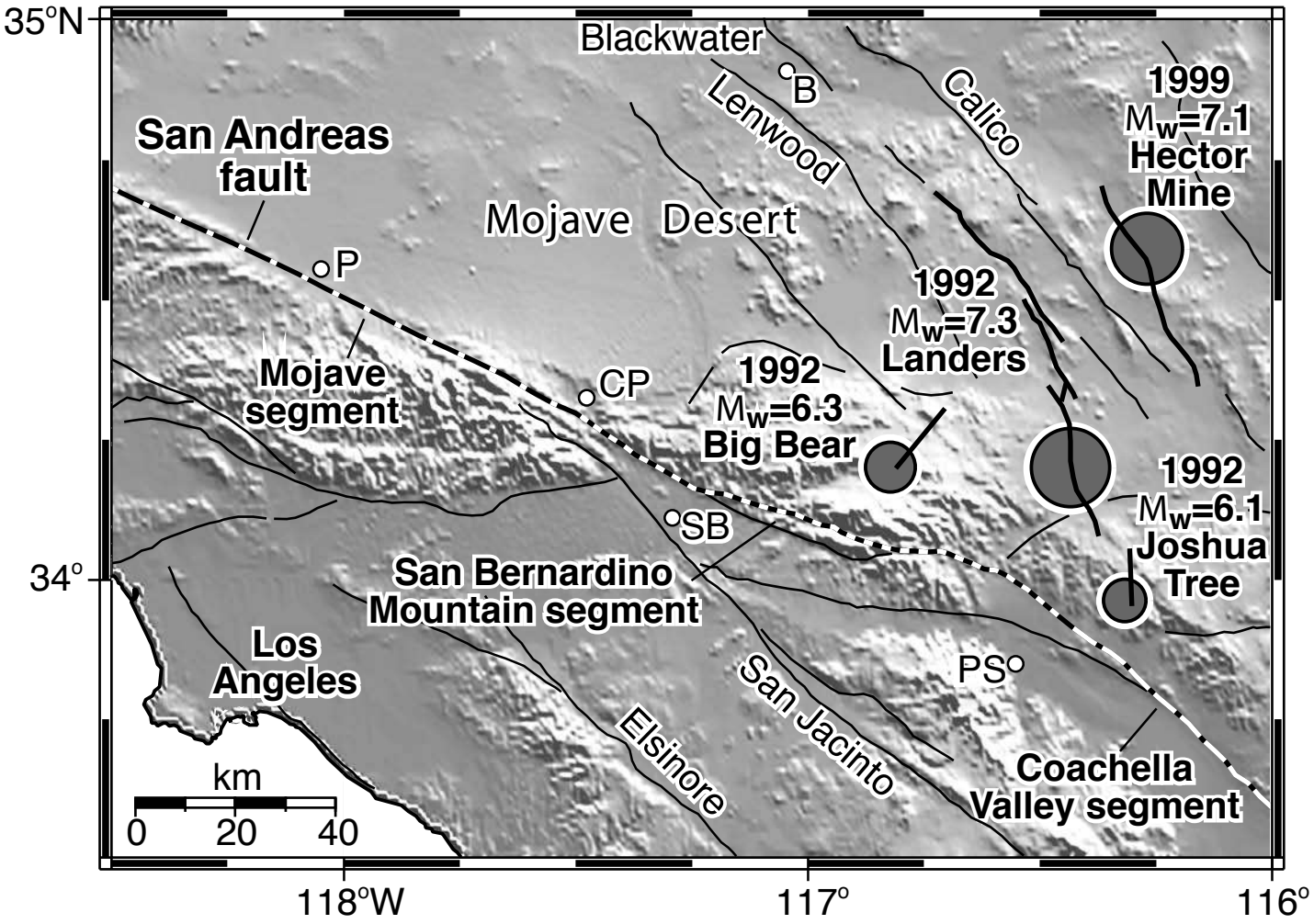
35°N
34°
118°W
117°
116°
Blackwater
B
Lenwood
Calico
1999
Mw=7.1
Hector
Mine
San Andreas
fault
Mojave Desert
P
1992
Mw=7.3
Landers
Mojave
segment
CP
1992
Mw=6.3
Big Bear
1992
Mw=6.1
Joshua
Tree
SB
San Bernardino
Mountain segment
Los
Angeles
PS
San Jacinto
Elsinore
Coachella
Valley segment
km
0
20
40

Fig. 1

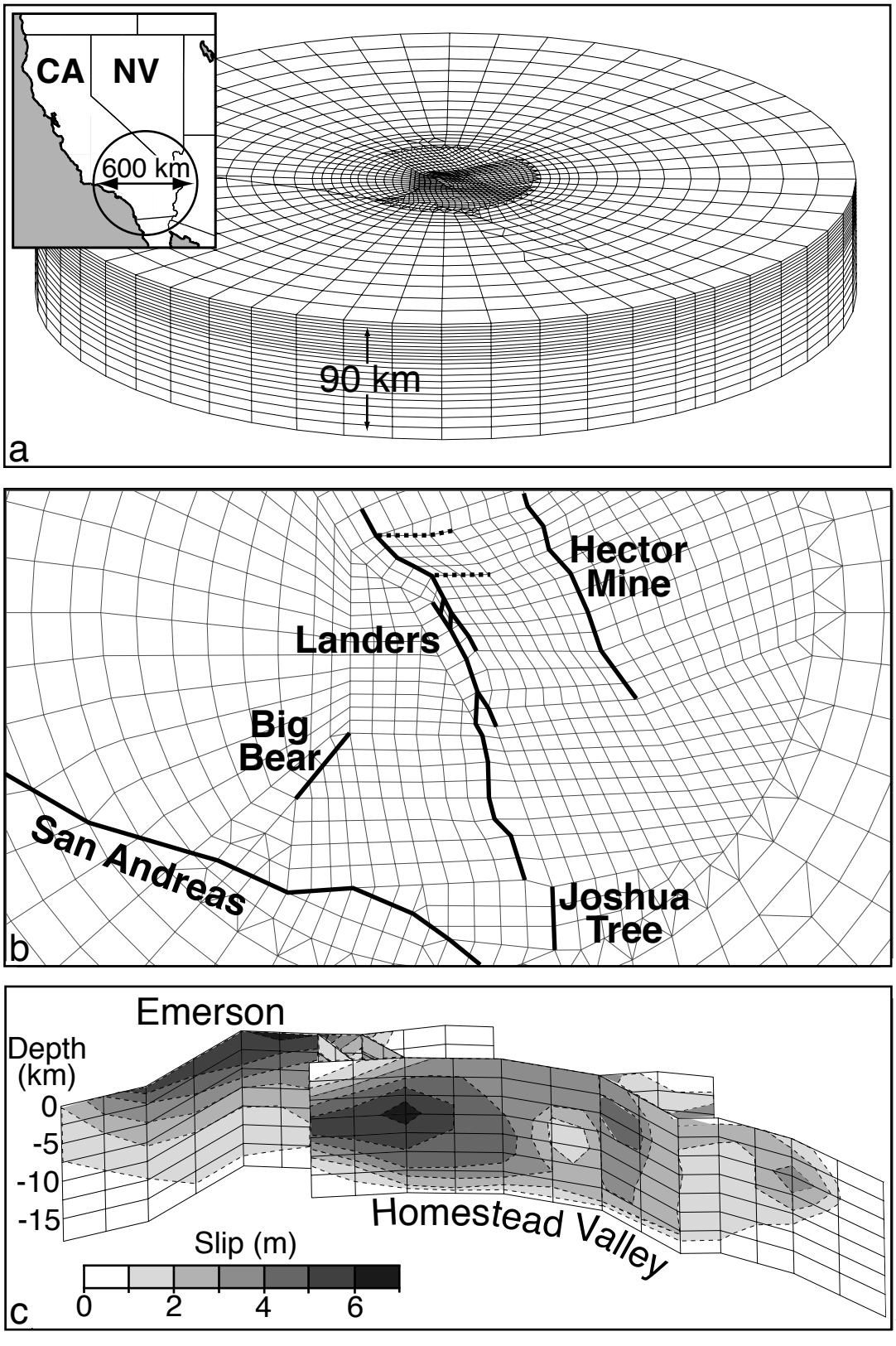
CA
NV
600 km
90 km
a
Hector
Mine
Landers
Big
Bear
San Andreas
Joshua
Tree
b
Emerson
Depth
(km)
0
-5
-10
-15
Homestead Valley
Slip (m)
0
2
4
6
c

Fig. 2

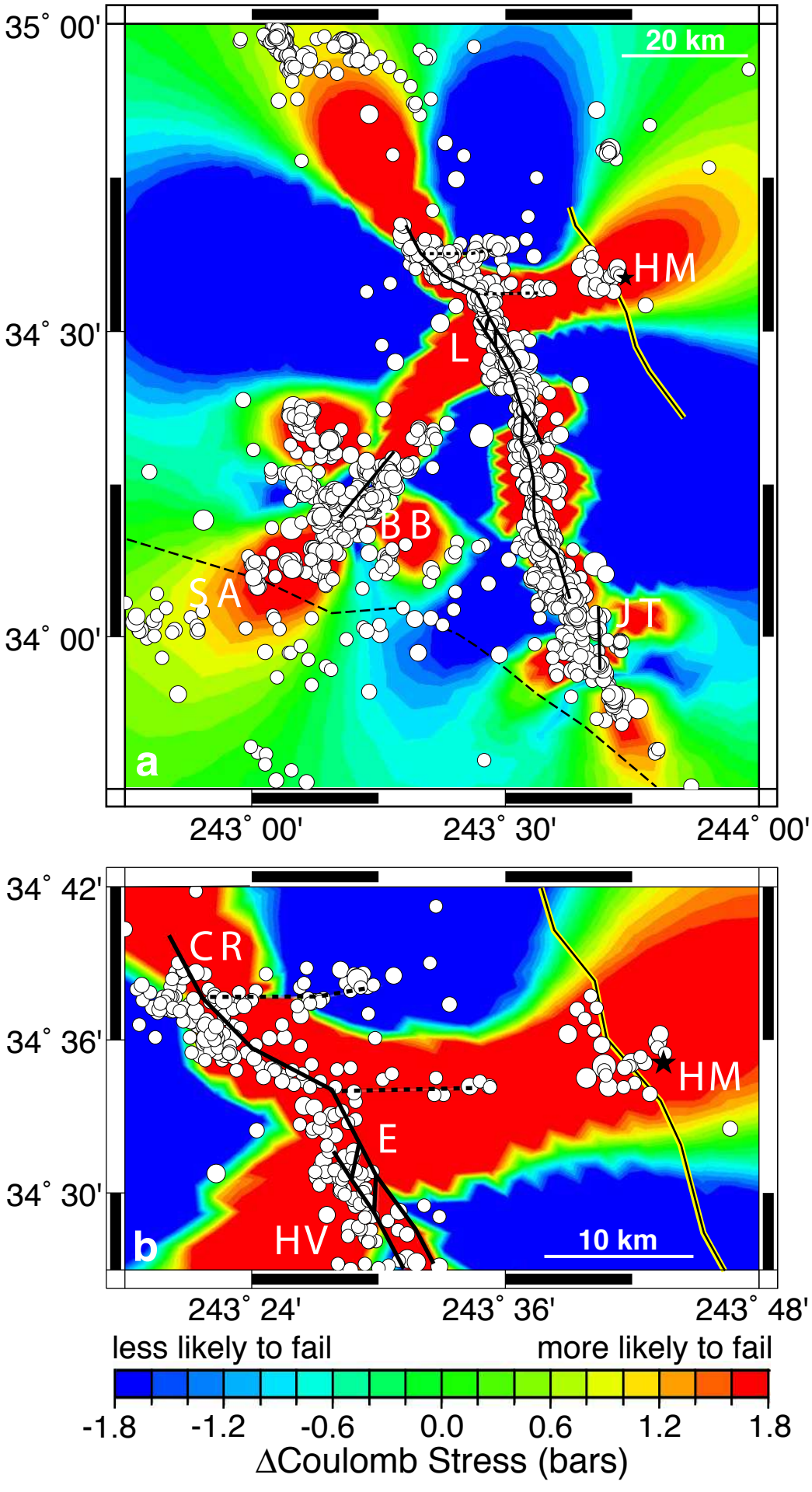
35° 00'
34° 30'
34° 00'
20 km
HM
L
B B
S A
J T
a
243° 00'
243° 30'
244° 00'
34° 42'
34° 36'
34° 30'
C R
HM
E
HV
b
10 km
243° 24'
243° 36'
243° 48'
less likely to fail
more likely to fail
-1.8
-1.2
-0.6
0.0
0.6
1.2
1.8
ΔCoulomb Stress (bars)

Fig. 3

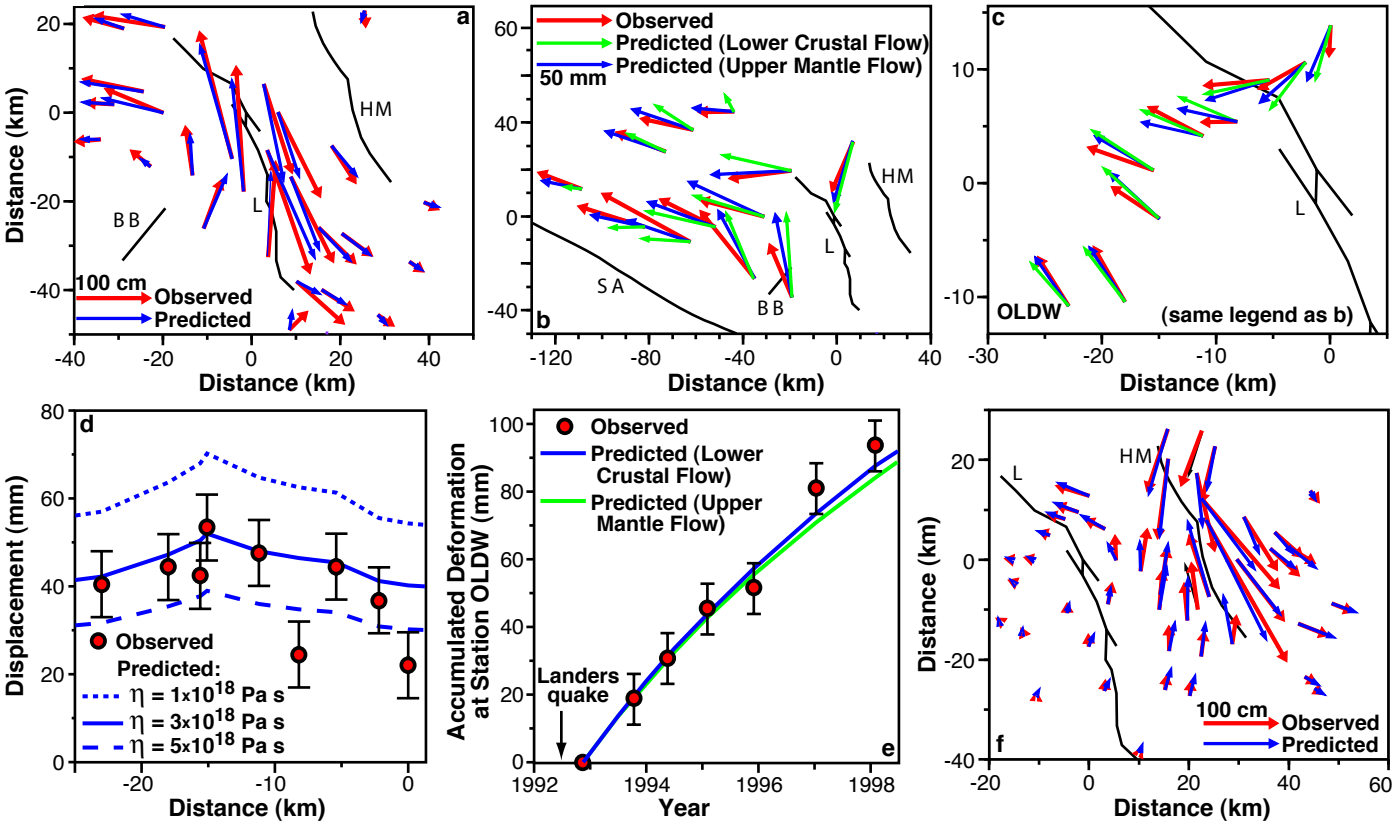
a
Distance (km)
Distance (km)
HM
BB
L
100 cm
Observed
Predicted
b
Observed
Predicted (Lower Crustal Flow)
Predicted (Upper Mantle Flow)
50 mm
HM
L
SA
BB
Distance (km)
c
L
OLDW
(same legend as b)
Distance (km)
d
Displacement (mm)
Observed
Predicted:
η = 1x10^18 Pa s
η = 3x10^18 Pa s
η = 5x10^18 Pa s
Distance (km)
Accumulated Deformation at Station OLDW (mm)
Observed
Predicted (Lower Crustal Flow)
Predicted (Upper Mantle Flow)
Landers quake
e
Year
Distance (km)
L
HM
100 cm
Observed
Predicted
f
Distance (km)

Fig. 4

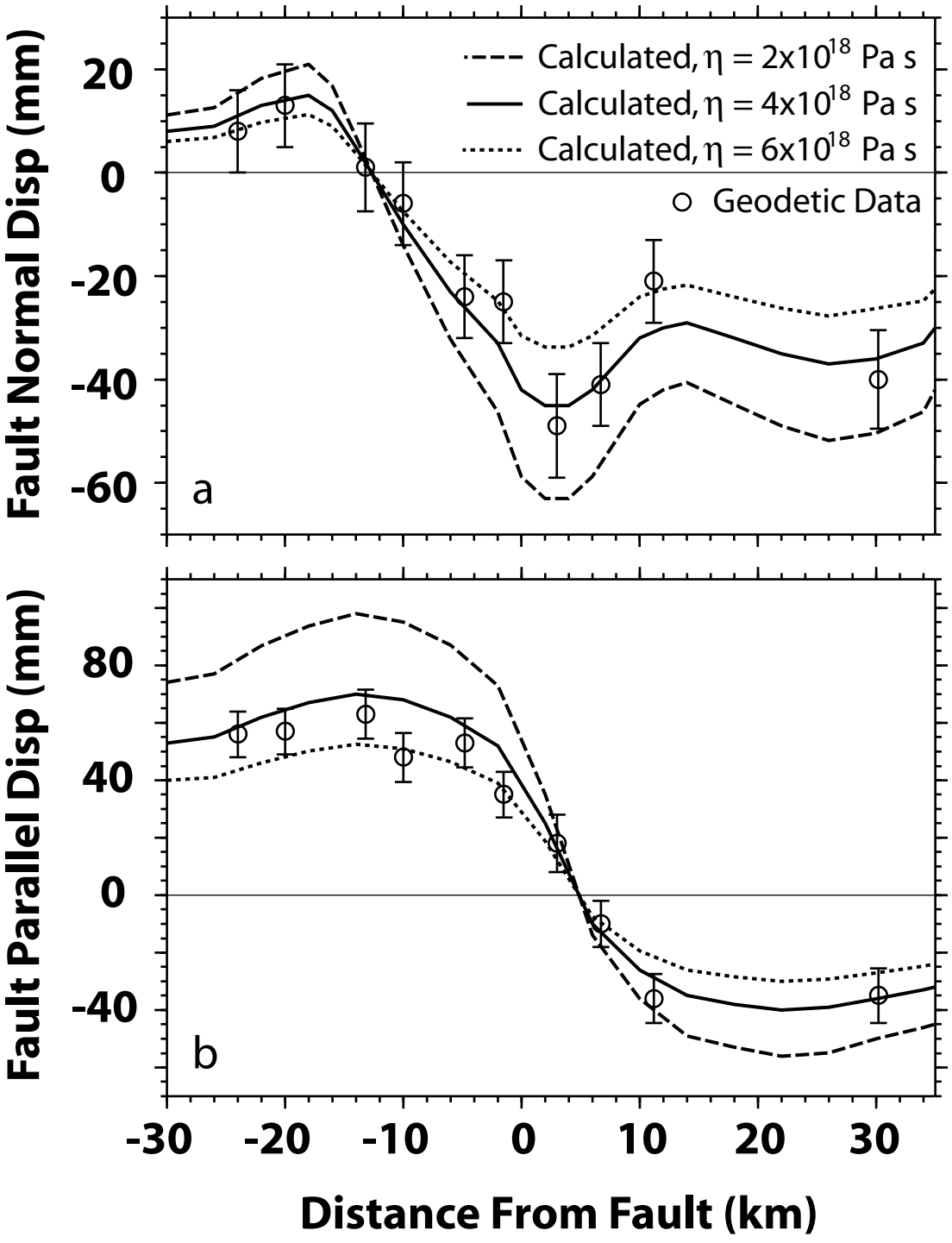
Calculated, η = 2x10^18 Pa s
Calculated, η = 4x10^18 Pa s
Calculated, η = 6x10^18 Pa s
Geodetic Data
Fault Normal Disp (mm)
20
0
-20
-40
-60
a
Fault Parallel Disp (mm)
80
40
0
-40
b
-30
-20
-10
0
10
20
30
Distance From Fault (km)

Fig. 5

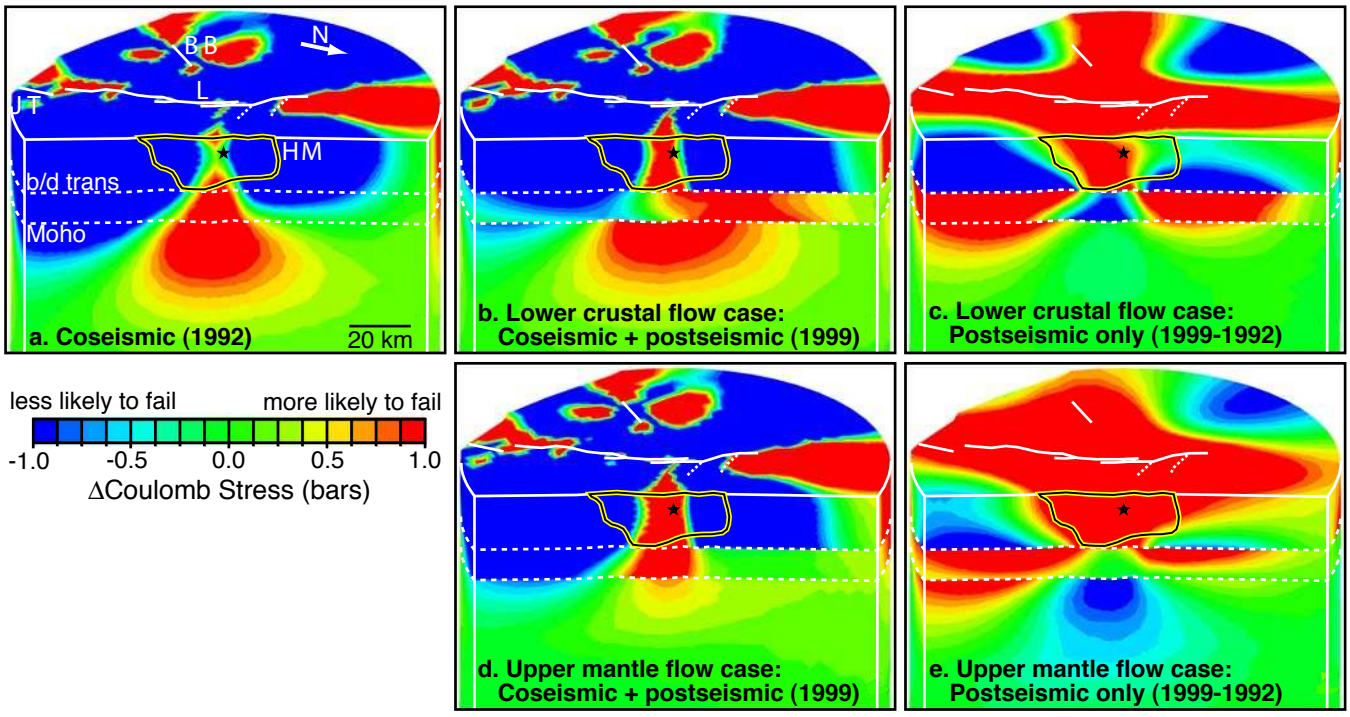
BB
N
L
HM
b/d trans
Moho
a. Coseismic (1992)
20 km
b. Lower crustal flow case:
Coseismic + postseismic (1999)
c. Lower crustal flow case:
Postseismic only (1999-1992)
less likely to fail
more likely to fail
-1.0
-0.5
0.0
0.5
1.0
ΔCoulomb Stress (bars)
d. Upper mantle flow case:
Coseismic + postseismic (1999)
e. Upper mantle flow case:
Postseismic only (1999-1992)

Fig. 6

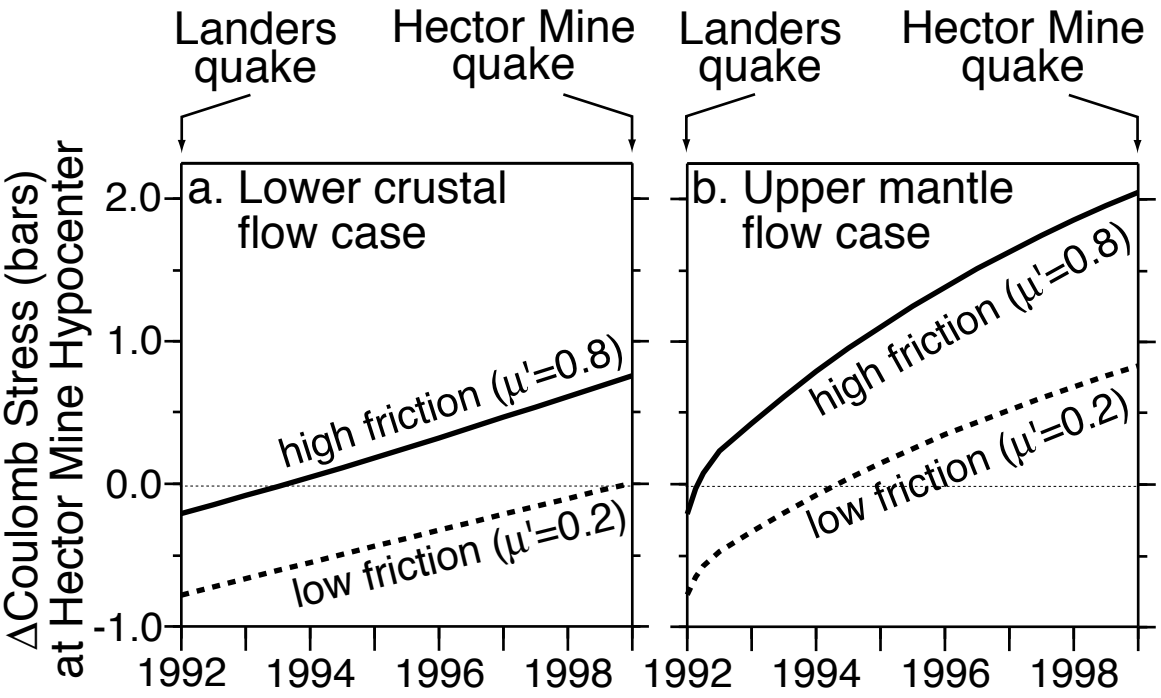
Landers quake
Hector Mine quake
Landers quake
Hector Mine quake
ΔCoulomb Stress (bars) at Hector Mine Hypocenter
a. Lower crustal flow case
b. Upper mantle flow case
high friction (μ'=0.8)
low friction (μ'=0.2)
high friction (μ'=0.8)
low friction (μ'=0.2)
2.0
1.0
0.0
-1.0
1992
1994
1996
1998
1992
1994
1996
1998

Fig. 7

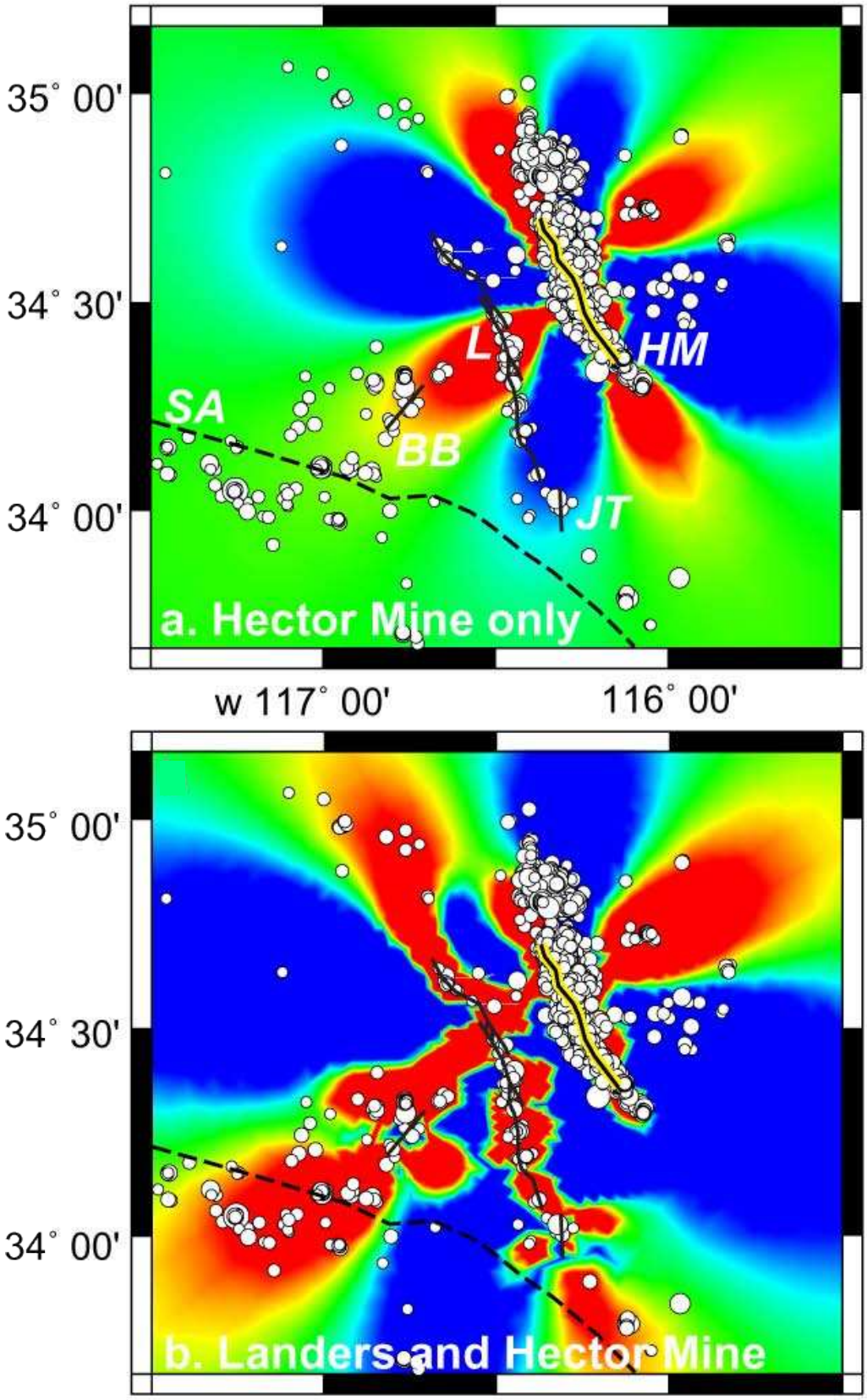
35° 00'
34° 30'
34° 00'
L
HM
SA
BB
JT
a. Hector Mine only
w 117° 00'
116° 00'
35° 00'
34° 30'
34° 00'
b. Landers and Hector Mine

Fig. 8

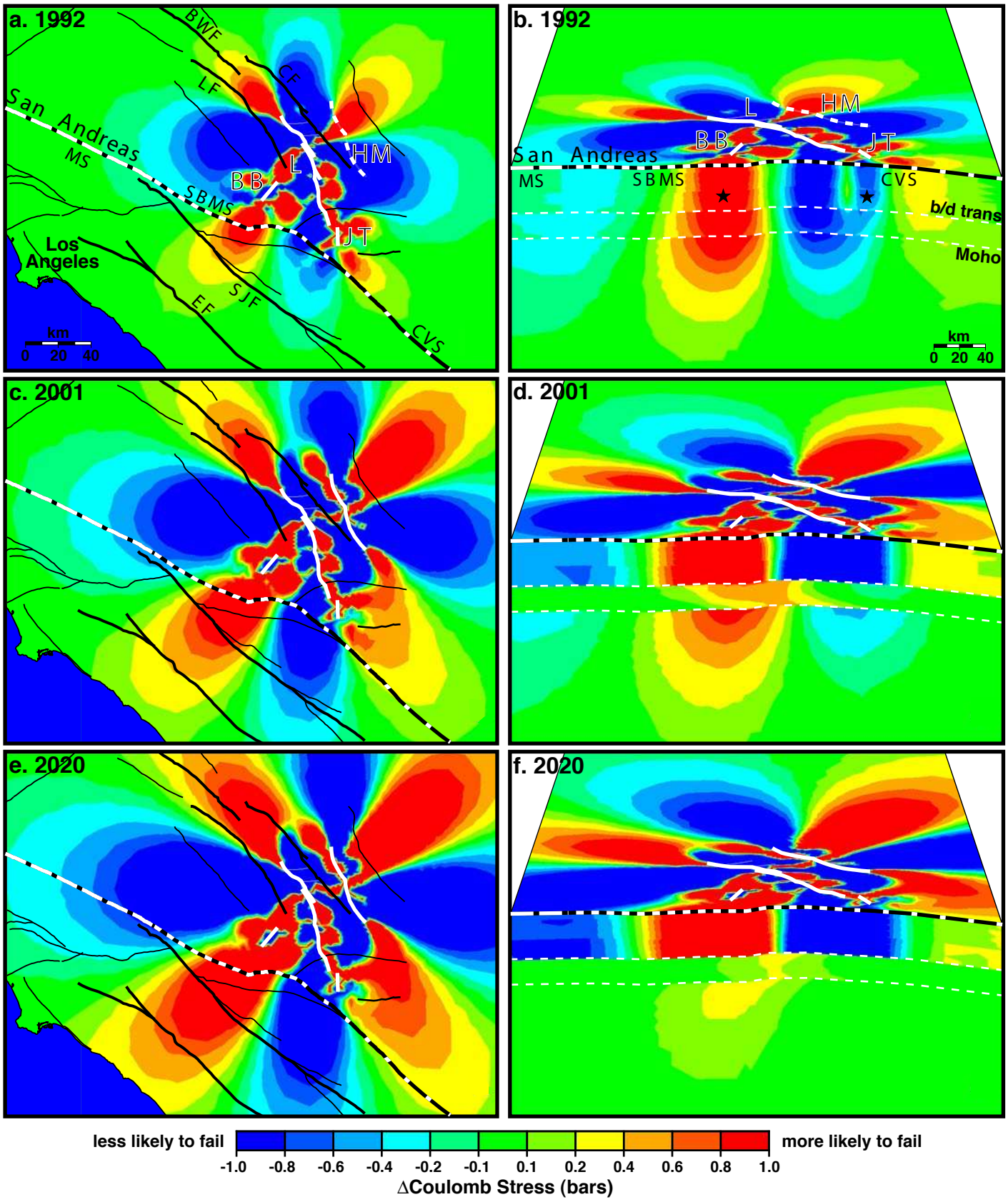
a. 1992
BWF
LF
CF
San Andreas
MS
SBMS
BB
L
HM
JT
Los Angeles
EF
SJF
CVS
km
0 20 40
b. 1992
L
HM
BB
JT
San Andreas
MS
SBMS
CVS
b/d trans
Moho
km
0 20 40
c. 2001
d. 2001
e. 2020
f. 2020
less likely to fail
more likely to fail
-1.0 -0.8 -0.6 -0.4 -0.2 -0.1 0.1 0.2 0.4 0.6 0.8 1.0
ΔCoulomb Stress (bars)

Fig. 9

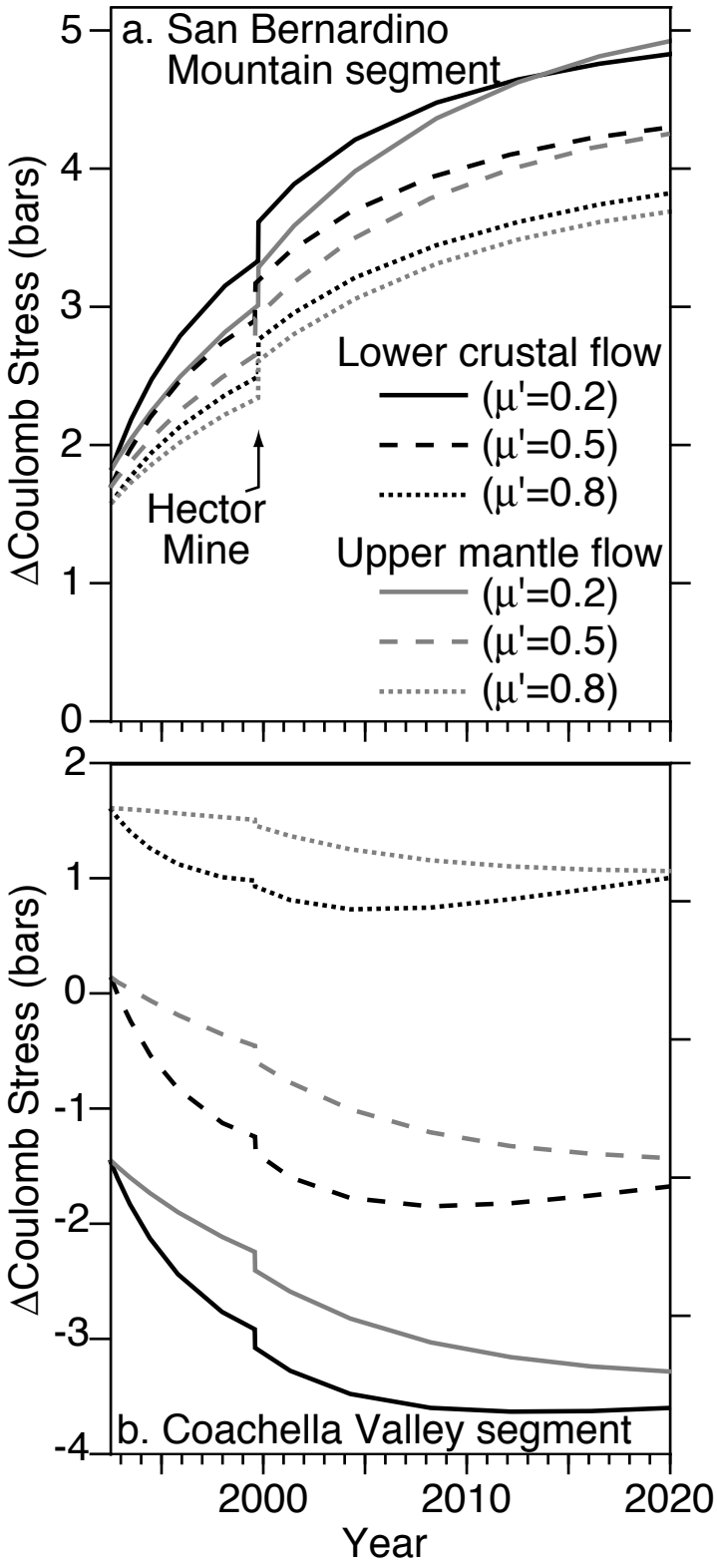
a. San Bernardino
Mountain segment
ΔCoulomb Stress (bars)
5
4
3
2
1
0
Lower crustal flow
(μ'=0.2)
(μ'=0.5)
(μ'=0.8)
Upper mantle flow
(μ'=0.2)
(μ'=0.5)
(μ'=0.8)
Hector
Mine
2
1
0
-1
-2
-3
-4
b. Coachella Valley segment
2000
2010
2020
Year

Fig. 10

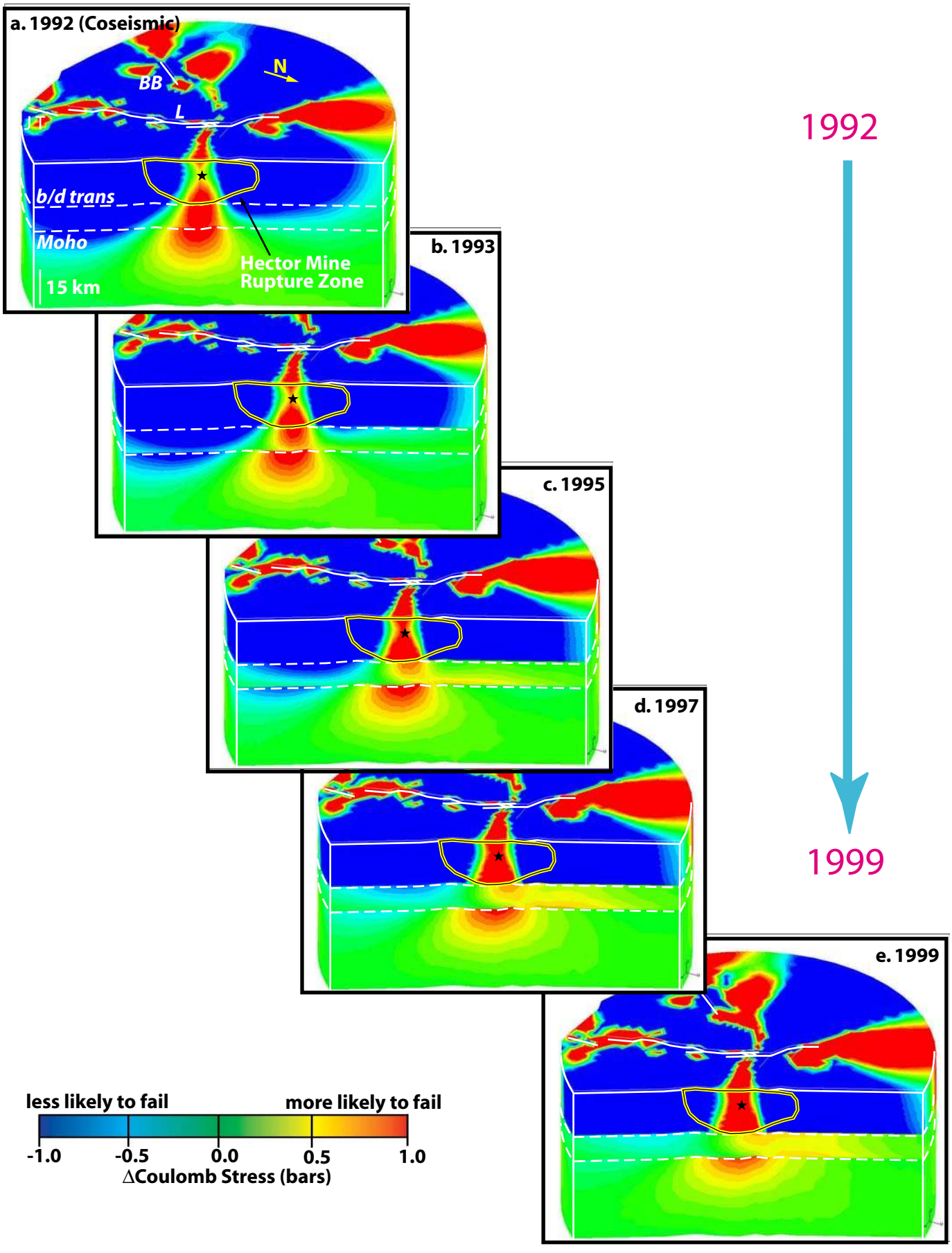
a. 1992 (Coseismic)
BB
L
N
b/d trans
Moho
15 km
Hector Mine
Rupture Zone
b. 1993
c. 1995
d. 1997
e. 1999
1992
1999
less likely to fail
more likely to fail
-1.0
-0.5
0.0
0.5
1.0
ΔCoulomb Stress (bars)

Fig. 11

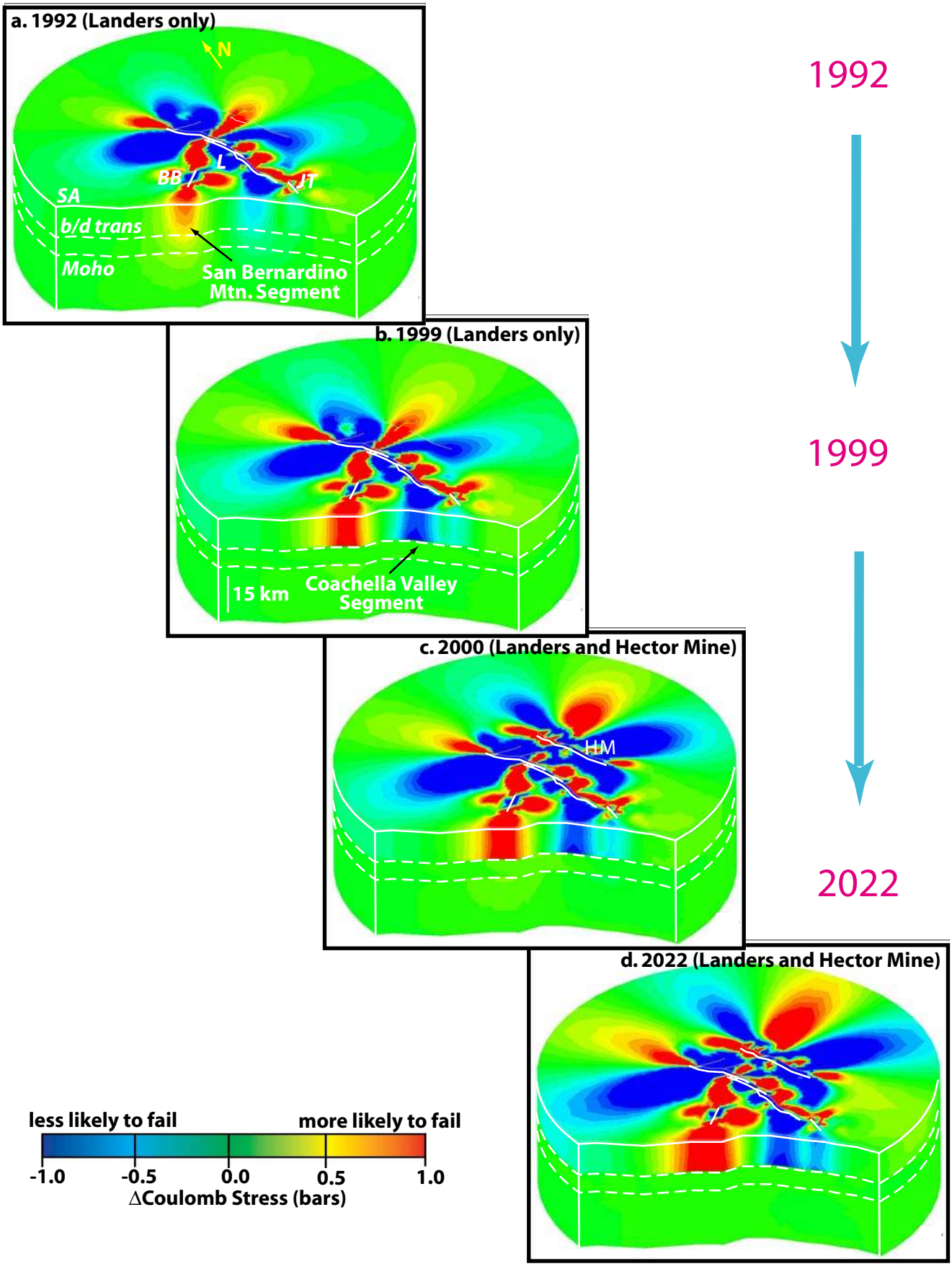
a. 1992 (Landers only)
N
L
BB
JT
SA
b/d trans
Moho
San Bernardino Mtn. Segment
b. 1999 (Landers only)
15 km
Coachella Valley Segment
c. 2000 (Landers and Hector Mine)
HM
d. 2022 (Landers and Hector Mine)
1992
1999
2022
less likely to fail
more likely to fail
-1.0
-0.5
0.0
0.5
1.0
ΔCoulomb Stress (bars)

Fig. 12